Cyanine-loaded lipid nanoparticles for improved *in vivo* fluorescence imaging

Isabelle Texier
Mathieu Goutayer
Anabela Da Silva
Laurent Guyon
Nadia Djaker
Commissariat à l'Énergie Atomique
LETI-DTBS
17 rue des Martyrs
Grenoble Cedex, 38054
France
E-mail: isabelle.texier-nogues@cea.fr

Véronique Josserand
Institut Albert Bonniot
INSERM U823
La Tronche, 38706
France

Emmanuelle Neumann
IBS J.-P. Ebel
UMR 5075 CNRS-CEA-UJF
41 rue Jules Horowitz
Grenoble Cedex 1, 38027
France

Jérôme Bibette
Ecole Supérieure de Physique et de Chimie Industrielles de la Ville de Paris
Laboratoire des colloïdes et matériaux divisés
10 rue Vauquelin
Paris Cedex 5, 75231
France

Françoise Vinet
Commissariat à l'Énergie Atomique
LETI-DTBS
17 rue des Martyrs
Grenoble Cedex, 38054
France

Abstract. Fluorescence is a very promising radioactive-free technique for functional imaging in small animals and, in the future, in humans. However, most commercial near-infrared dyes display poor optical properties, such as low fluorescence quantum yields and short fluorescence lifetimes. In this paper, we explore whether the encapsulation of infrared cyanine dyes within the core of lipid nanoparticles (LNPs) could improve their optical properties. Lipophilic dialkylcarbocyanines DiD and DiR are loaded very efficiently in 30–35-nm-diam lipid droplets stabilized in water by surfactants. No significant fluorescence autoquenching is observed up to 53 dyes per particle. Encapsulated in LNP, which are stable for more than one year at room temperature in HBS buffer (HEPES 0.02 M, EDTA 0.01 M, pH 5.5), DiD and DiR display far improved fluorescence quantum yields Φ (respectively, 0.38 and 0.25) and longer fluorescence lifetimes τ (respectively, 1.8 and 1.1 ns) in comparison to their hydrophilic counterparts Cy5 (Φ=0.28, τ=1.0 ns) and Cy7 (Φ=0.13, τ=0.57 ns). Moreover, dye-loaded LNPs are able to accumulate passively in various subcutaneous tumors in mice, thanks to the enhanced permeability and retention effect. These new fluorescent nanoparticles therefore appear as very promising labels for *in vivo* fluorescence imaging. [DOI: 10.1117/1.3213606]

Keywords: fluorescence imaging; lipid nanoparticles; cyanine dyes; molecular imaging; in vivo imaging; fluorescence quantum yield; fluorescence lifetime.

Paper 09114R received Mar. 30, 2009; revised manuscript received Jun. 30, 2009; accepted for publication Jul. 7, 2009; published online Sep. 8, 2009.

1 Introduction

Small animal fluorescence imaging has emerged in the last few years and is assessed nowadays as a very promising technique for drug discovery and development.[1–3] Human diagnostic applications are now envisionned.[4–6] This next step necessitates fluorescent probes with improved sensitivity and selectivity to respond to the high constraints imposed by the absorption and diffusion properties of the living tissues. The specifications that should fulfill the fluorescent labels are: (*i*) absorb/emit in the near-infrared window (650–900 nm) for which tissue absorption and diffusion are reduced; (*ii*) have a high fluorescence quantum yield for sensitivity detection; (*iii*) have a suitable fluorescence lifetime in the 1–5 ns range whenever time-resolved imaging is envisioned; (*iv*) have a suitable pharmacokinetics for signal selectivity and subsequent elimination of the probe after imaging.

Two main classes of fluorescent tracers for *in vivo* fluorescence imaging exist: near-infrared organic dyes and semiconductor nanocrystals ("quantum dots"). Quantum dots display interesting optical properties, such as a narrow and symmetric emission band, which can be tuned in the near-infrared domain by the size and composition of the nanocrystal core, a long luminescence lifetime (10–100 ns, typically), and a good photostability.[7–9] However, even if new compositions

Address all correspondence to: Isabelle Texier, LETI DTBS, CEA, 17 rue des martyrs-Grenoble, 38054 France; Tel: +33 438 784 670; Fax: +33 438 785 787; E-mail: isabelle.texier-nogues@cea.fr

1083-3668/2009/14(5)/054005/11/$25.00

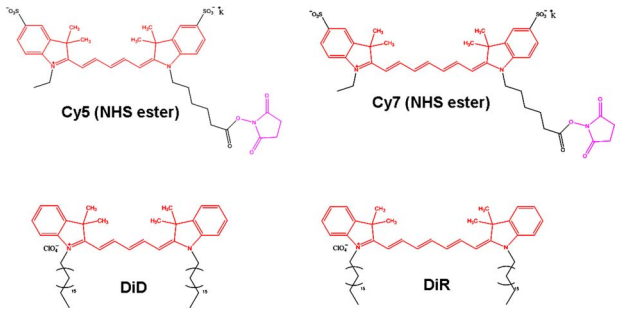

Fig. 1 Structure of the hydrophilic Cy5 and Cy7 cyanines, as well as their lipophilic counterparts DiD and DiR.

are presently under development, their inorganic core most often contains heavy metal with acute or chronic toxicity (Cd, Se, Te, etc.), and the use of organic biodegradable molecules is to be preferred. Consequently, molecular organic dyes have been extensively studied and developed in the last few years.[10–17] For the near-infrared domain, the choice of organic dyes is mainly restricted to the cyanine structure.[11] However, fluorescence quantum yields and fluorescence lifetimes of cyanines, as well as their solubility, decrease when shifting from the visible to the near infrared (see, for example, Cy5 and Cy7, Fig. 1, Table 1).[10,18] Most efforts in the development of new near-infrared cyanine dyes have been focused on increasing their solubility, mainly by the introduction of sulfonate, saccharide or polyoxyethylene groups,[10,15–17] or their chemical stability, for example, by the rigidification of the polymethine chain.[12,13] More recently, Lee et al. have worked on the fluorescence lifetime engineering of cyanines in relation to their structure.[19] However, despite improved solubility and fluorescence quantum yields, most commercial near-infrared dyes still display very low fluorescence quantum yields (<0.1) and short fluorescence lifetimes (1 ns or less) in aqueous buffers.

The encapsulation of organic dyes in molecular capsules,[20] or organic,[21–29] or inorganic[30–32] nanoparticles has been proposed in order to improve the optical properties of the fluorophores (mainly increase their fluorescence quantum yield and their chemical and photochemical stabilities). Nanoparticular platforms appear more versatile than molecular scaffolds for the design of multifunctional structures. Moreover, passive accumulation in tumor areas has been reported for a variety of nanomaterials. It is accounted for by the increased porosity in the tumor vasculature, along with the low lymphatic drainage of the tumors, in comparison to the healthy tissues [enhanced permeability and retention (EPR) effect].[33] Even if fenestrations of the vasculature at the tumor sites strongly depend on tumor models,[34] 20–100 nm often appears as an optimal diameter for an efficient extravasation and retention of the nanoparticles from capillaries to the tumor interstitial tissues.[35] Molecular structures with a lower molecular weight would not benefit from the EPR effect.

Inorganic matrixes for dye encapsulation encompass mainly silica[31,32,36] and, more recently, calcium phosphate[30] nanoparticles. The organic dyes can be included in, or preferentially covalently linked to, the matrix in order to avoid dye

Table 1 Optical properties of DiD and DiR in methanol or encapsulated in lipid nanoparticles of different compositions or with different loading ratio. The fluorescent properties of Cy5 and Cy7, hydrophilic counterparts of, respectively, DiD and DiR, are also listed for comparison. All the data are recorded in 1 X PBS, except for the DiD and DiR dyes dissolved in methanol.

Dye	λ_{abs}^{max} (nm)	λ_{em}^{max} (nm)	Half-life[a] (h)	Φ[b]	τ (ns)[c]	k_r ($\times 10^8$ s^{-1})	k_{nr} ($\times 10^8$ s^{-1})
Cy5, PBS	646	663	37	0.28	0.98±0.03	2.9±0.2	7.3±0.6
DiD, MeOH	644	665	531	0.33	1.1±0.05	3.0±0.3	6.1±0.6
DiD, formulation A1,[d] 4 dyes/part.	646	668	—	0.38	1.88±0.03	2.1±0.1	3.4±0.3
DiD, formulation A1,[d] 21 dyes/part.	646	668	64	0.37	1.82±0.03	2.0±0.1	3.5±0.3
DiD, formulation A1,[d] 53 dyes/part.	646	668	—	0.35	1.75±0.03	2.0±0.1	3.7±0.3
DiD, formulation A2,[e] 21 dyes/part.	646	668	—	0.37	1.98±0.05	1.9±0.1	3.2±0.3
DiD, formulation B2,[f] 21 dyes/part.	646	668	—	0.38	2.09±0.05	1.8±0.1	3.0±0.3
DiD, formulation C2,[g] 21 dyes/part.	646	668	—	0.36	2.09±0.05	1.7±0.1	3.1±0.3
Cy7, PBS	749	774	—	0.13	0.57±0.03	2.3±0.2	15.3±1.2
DiR, MeOH	747	774	—	0.28	1.1±0.05	2.5±0.2	6.5±0.7
DiR, formulation A1,[d] 21 dyes/part.	748	775	—	0.25	1.1±0.1	2.3±0.3	6.8±1.0

[a]Half-lives of the dyes are calculated using a linear fit of the photobleaching curves (Fig. 6);
[b]the estimated error on the values is 5%;
[c]standard deviations are obtained using different monoexponential fitting of the data (correlation coefficient $\chi^2<1.2$);
[d]formulation A1: core composition 3:1 Suppocire:soybean oil, surfactant layer composition 2:1 lecithine:Myrj 53, 35 nm diam;
[e]formulation A2: core composition 3:1 Suppocire:soybean oil, surfactant layer composition 1:1 lecithine:Myrj 53, 30 nm diam;
[f]formulation B2: core composition 100% Suppocire, surfactant layer composition 1:1 lecithine:Myrj 53, 30 nm diam;
[g]formulation C2: core composition 1:3 Suppocire:soybean oil, surfactant layer composition 1:1 lecithine:Myrj 53, 30 nm diam.

leaching. Improved fluorescence quantum yields and resistance to photobleaching are generally observed and attributed to the shielding effect of the matrix from oxygen or solvent quenching. The encapsulation impact on the dye fluorescence lifetimes is however more complicated, dependant on the dye concentration and nanoparticule architecture.[36–39] Surprisingly, until very recently, very few organic-based nanoparticles encapsulating organic dyes and especially designed for noninvasive *in vivo* fluorescence imaging had been described. This is surprising because these organic nanocarriers, such as liposomes, micelles, and dendrimers, have been very extensively studied for several years for drug-delivery purposes. However, the use of organic drug-delivery systems encapsulating dyes and designed especially for fluorescence imaging has been described in the last two years for different nanocarriers, such as polymers,[28,29] dendrimers,[24,25] micelles,[27] liposomes,[26] polymersomes,[22] lipoproteins,[23] and bacteriophage particles.[21]

We here describe new lipid nanoparticles (LNPs) able to efficiently encapsulate lipophilic compounds for drug delivery and imaging purposes. These new formulations are based on the use of cheap, generally recognized as safe (GRAS) components, such as soybean oil, lecithin, and polyoxyethylene surfactants, and are manufactured very easily using sonication. They display ≈30–35 nm hydrodynamic diameter and a very long colloidal stability (>1 y) at room temperature in aqueous buffer. Their oily core (made from a mixture of vegetable oil and a wax, Suppocire™) therefore provides a very stable locally viscous and nonpolar medium, dispersed in aqueous buffer. Medium polarity and viscosity are parameters known to influence the fluorophore optical properties, in particular, fluorescence quantum yields and fluorescence lifetimes.[18] We therefore investigate whether the encapsulation of lipophilic near-infrared cyanines within the core of LNP could increase the fluorescence quantum yields and lifetimes of the dyes and more generally improve their optical properties. Moreover, passive tumor targeting of dye-loaded LNPs is demonstrated in subcutaneous tumors bearing mice.

2 Materials and Methods

2.1 *Preparation of Dye-Loaded Lipid Nanoparticles*

Suppocire NC™ is a kind gift from Gattefossé (Saint-Priest, France). Myrj 53™ (polyethylene glycol 50 stearate) is from Croda Uniqema (Chocques, France), and DiD and DiR dyes from Invitrogen. Soybean oil, L-α-lecithin (soybean lecithin at >30% of phosphatidylcholine), and other chemical products are purchased from Sigma Aldrich (Saint-Quentin Fallavier, France).

LNPs are composed of a lipid core (mixture of soybean oil and Suppocire NC), stabilized by a surfactant shell (L-α-lecithin and Myrj 53), and dispersed in an aqueous phase, as depicted in Fig. 2. For preparation of a 2-mL dispersion batch, 200 mg of the lipid components (150 mg of Suppocire NC™/50 mg of soybean oil for formulations A1 and A2, 200 mg of Suppocire NC for formulation B2, 50 mg of Suppocire NC/150 mg of soybean oil for formulation C2) are mixed with L-α-lecithin (138 mg for formulation A1, 100 mg for formulations A2, B2, C2) and the appropriate amount of dye dissolved in dichloromethane. After homogeneization at 45 °C, the organic solvent is evaporated under

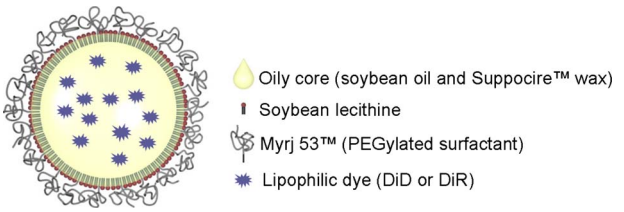

Fig. 2 Schematic representation of the dye-loaded LNP structure.

reduced pressure and the lipid phase is crudely mixed with the continuous aqueous phase composed of Myrj 53 (228 mg for formulation A1, 331 mg for formulations A2, B2, C2), 50 mg of glycerol, and the appropriate buffer [1X PBS (10 mM phosphate, 150 mM NaCl, pH 7.2) if not stated otherwise, qsp 2 mL]. Sonication (VCX750 Ultrasonic processor, power output 190 W, 3-mm probe diameter, Sonics) is performed at 40 °C for a whole 5-min period to yield 35 nm (formulation A1) or 30 nm (formulations A2, B2, C2) diameter particles. In order to eliminate free (nonencapsulated) DiD or DiR dyes and other components, LNP dispersions are dialyzed overnight at room temperature against 1000 times their volume in the appropriate aqueous buffer (12–14,000 Da MW cut off membranes, ZelluTrans). Finally, the LNP dispersion is filtered through a 0.22-μm Millipore membrane for sterilization before characterization and/or injection.

2.2 *Structural Characterizations*

Cryo-transmission electron microscopy (TEM) analysis is performed using an FEI CM200 microscope with a LaB_6 electron source operating at 200 kV. The sample is deposited onto a holey carbon grid, blotted to remove excess liquid, and frozen by plunging rapidly into liquid ethane at the temperature of liquid nitrogen. Grids are transferred to a Gatan 626 cryoholder and imaged by low-dose techniques, maintaining the low temperature (−185 °C) throughout. Images are recorded at a nominal magnification of 38,000x. Micrographs are recorded on Kodak SO-163 film and developed for 12 min in full-strength Kodak D19. The hydrodynamic diameter and zeta potential of the lipid nanoparticles are measured with a Malvern Zeta Sizer Nano instrument (NanoZS) in 0.1 X PBS buffer. Values indicate mean and standard deviation of at least three measures per batch, for three different batches per formulation.

2.3 *Steady-State Optical Characterizations*

The absorbance and fluorescence measurements are performed respectively using a Cary 300 Scan (Varian) UV-Visible spectrophotometer and a Perkin Elmer LS50B fluorimeter. The absolute fluorescence quantum yields Φ are calculated by comparison to standards of known Φ [Nile blue perchlorate in ethanol (Φ=0.27)[40] for 600-nm excitation (Cy5 and DiD), HITC in methanol (Φ=0.28)[41] for 700-nm excitation (Cy7 and DiR)]. A continuous increase of the absorbance with decreasing wavelengths (Absorbance $\propto\lambda^{-4}$) due to a slight Rayleigh scattering effect has been observed for unloaded LNPs. This effect is corrected for the calculation of the fluorescence quantum yields of the dyes whenever encapsulated in the nanocarriers. All steady-state characterizations are carried out using dye or particle dispersions in the

relevant buffers, with optical densities of 0.1–1 for absorbance measurements, and ≈0.1 for fluorescence measurements.

The efficiency of DiR and DiD encapsulation is measured by spectrophotometric titration, using the absorbance of the LNP dispersion before and after extensive dialysis. Encapsulation efficiencies of >99% are observed. An estimate of the average number of dyes per particle $\langle N \rangle$ is calculated based on the number of encapsulated dyes (n_f), and hypothesizing that the volume of the dispersed phase V_d (representing the total volume occupied by the n_p particles) include both the oily core and the surfactant shell. $\langle N \rangle$ is then obtained using the following formula:

$$\langle N \rangle = \frac{n_f}{n_p} = n_f \frac{v}{V_d} \tag{1}$$

in which v represents the volume of a particle measured by diffusion light scattering (30 or 35 nm diam), and V_d, the total volume (including oil, wax, lecithin, and pegylated surfactants) occupied by the n_p particles, is obtained using an average density of the dispersed phase of 1.1.

The photobleaching measurements are carried out with the same setup as mouse imaging, with an excitation power of 200 μW/cm^2 at 633 nm. Then, 10 μM free or encapsulated dye solutions are prepared in the appropriate medium (100 μL) and introduced into glass capillaries that are simultaneously lightened in the homogeneous lightening field (homogeneity >95% in 20 cm^2). Half-lives of the dyes in the different conditions are calculated using a linear fit of the photobleaching curves.

2.4 *Lifetime Measurements*

Fluorescence lifetime measurements are carried out in plastic cuvettes with ≈0.1 absorbance solutions at the excitation wavelength, using a time-correlated single-photon counting (TCSPC) setup. For DiD and Cy5, the excitation source is a 630-nm laser diode (BHL-600, Becker&Hickl) operating at 50 MHz (150 μW, 80-ps pulses). For DiR and Cy7, the excitation source is a Ti:Sa femtosecond laser (Tsunami, Spectra-Physics) operating at 730 nm and 80 MHz (10 mW, 100-fs pulses broaden to a few picoseconds after propagation in an optical fiber). The detection of the emission signal, filtered by a RG665 (Cy5 and DiD) or a RG780 (Cy7 and DiR) filter (Schott), is carried out at right angle using a photomultiplier R3809U-50 (Hamamatsu), an amplifier UFAC-26 (Becker&Hickl), and the TCSPC module SPC-730 (Becker&Hickl). The fluorescence decays are analyzed using the SPCM software (Becker&Hickl), after deconvolution of the instrument response function. Monoexponential decay is used to fit recorded data, eventually taking into account a scattering contribution.

2.5 *Numerical Simulations*

In order to illustrate the benefit for *in vivo* imaging of developing fluorescent probes with long lifetimes, together with high quantum yields, a series of simulations are provided later (Fig. 8). To stay as close as possible to an actual situation, we consider a digitized 3-D volume of a living mouse acquired with a system previously described.[42] Inside this volume, a fluorescence object has been introduced (ellipsoid, semiaxes length: X: 1 cm, Y: 0.25 cm, Z: 0.1 cm). Fluorescence light propagation through biological tissues is usually modeled within the diffusion approximation as a two-step light-propagation phenomenon.[43] Suppose a diffusing medium, in the present case a mouse, with a total volume Ω and bounded by the surface $\partial\Omega$. Suppose a pointlike source located at the position $\mathbf{r}_s$ inside the diffusing medium with intensity $Q_o(\mathbf{r}_s)$. The fluorochromes present within the medium are excited by the incident diffuse photon density wave (DPDW) u_x at the excitation wavelength λ_x. Each excited fluorescent particle then acts as a secondary point source and gives birth to a fluorescent DPDW, propagating with a larger wavelength λ_m. This is commonly modeled, within the diffusion approximation, by the following set of weakly coupled partial differential equations:

$$\begin{cases} \dfrac{1}{c_n}\dfrac{\partial u_x(\mathbf{r},t)}{\partial t} + \nabla \cdot [-D_x(\mathbf{r}) \nabla u_x(\mathbf{r},t)] + \mu_{ax}(\mathbf{r}) u_x(\mathbf{r},t) = Q_O(\mathbf{r}_s,t) \\ \dfrac{1}{c_n}\dfrac{\partial u_m(\mathbf{r},t)}{\partial t} + \nabla \cdot [-D_m(\mathbf{r}) \nabla u_m(\mathbf{r},t)] + \mu_{am}(\mathbf{r}) u_m(\mathbf{r},t) = \beta(\mathbf{r}) \displaystyle\int_0^t \exp\left(\frac{-(t-t')}{\tau(\mathbf{r})}\right) u_x'(\mathbf{r},t')dt' \end{cases} . \tag{2}$$

The first equation represents the propagation of the excitation light (subscript x), from the pointlike source, located at position $\mathbf{r}_s$, to the fluorochrome at a position $\mathbf{r}$ inside the diffusing volume Ω. The second equation models the generation and the propagation of the emitted light (subscript m). u_m is the photon density of the emitted light. The coefficient $\mu_{ax}(\mathbf{r})$ [respectively, $\mu_{am}(\mathbf{r})$] is the absorption at the excitation (respectively, emission) wavelength due to the presence of both the local nonfluorescing chromophores and fluorochromes concentrations, at the excitation (respectively, emission) wavelength, c_n is the speed of light inside the medium. D_x (respectively, D_m) is the diffusion constant at the excitation (respectively, emission) wavelength. The parameter $\beta(\mathbf{r})$ involved in the fluorescence source term is the conversion factor of the excitation light at a point $\mathbf{r}$ into fluorescence light and depends on intrinsic properties of the fluorochromes, such as the fluorescence lifetime $\tau(\mathbf{r})$, the quantum yield, and also their local concentration. $\beta(\mathbf{r})$ is directly proportional to the

local concentration and represents a sensor of the position of the fluorochromes. Equations (2) are subject to the Robin boundary conditions, to be satisfied at the boundaries of the system $\partial\Omega$; however, it is usually admitted that this is equivalent to apply Dirichlet boundary conditions on boundaries situated at an extrapolated distance (dilatation of the volume due to the optical properties).

For simplicity, the optical properties are supposed to be the same at both the excitation and emission wavelengths: $D_x = D_m = D = 0.033$ cm and $\mu_{ax} = \mu_{am} = \mu_a = 0.3$ cm^{-1}, and the different subdomains are supposed to be homogeneous. The source is modeled as a sphere with radius 0.05 cm, located at position (0,0,0). The resolution of the equations is performed using the finite element method with the commercial software Comsol Multiphysics®. To that purpose, the volume has been meshed resulting in 20,844 deg of freedom. The chosen linear system solver is GMRES with a geometric multigrid preconditioner. The calculation is performed within the time interval [0; 12 ns], corresponding to usual time-resolved measurements, and the time stepping is 0.1 ns. The background lifetime is set to $\tau_0 = 0.5$ ns, and the fluorescence inclusion lifetime (0.5, 1.1, 1.8, 2.1, 5, 10 ns), as well as its concentration relative to background (background:inclusion 1:5 and 1:50) are varied.

2.6 *Animal Models*

Ts/Apc cells (murine breast carcinoma) are cultivated in RPMI 1640 medium (Gibco) supplemented with 4.5 g/L glucose, 10% fetal calf serum, 1% glutamine, 50 U/mL penicillin, 50 mg/mL streptomycin, and 2.5×10^{-5} M 2-mercaptoethanol. Human ovarian adenocarcinoma OVCAR-3 cells are cultivated in RPMI 1640 medium supplemented with 20% fetal calf serum, 1% glutamine, 50 U/mL penicillin, and 50 mg/mL streptomycin. All cell lines are cultured in 75-cm^3 flasks with 15 mL of growth medium and kept at 37 °C in a humidified 95% air/5% CO_2 atmosphere.

All the animal experiments are performed in agreement with the EEC and U.S. guidelines.[44] About two weekes prior to imaging, 10^6–10^7 Ts/Apc or OVCAR-3 cells are implanted subcutaneously in anesthetized female six-to-eight-week-old Nude mice (Janvier, le Genest Saint Isle, France). Imaging is carried out whenever the tumor reaches about 6–8 mm diam. For imaging, 200 μL of DiD-loaded LNP, representing 10 nmol of dye (3.2 mg of oil, 5×10^{14} particles with a local DiD concentration of 1.55 mM) are injected in the tail vein of the anesthetized animals (isoflurane/air 1.5%) placed on a warm plate (37.5 °C). Animals are subsequently imaged at the desired time points using a fluorescence-reflectance-imaging setup. This homemade system is adapted from the commercially available Aequoria™ system from Hamamatsu. It is made up of a dark box equipped with a mouse-body temperature controller and a gas anesthesia device. The excitation device is composed of 10 LED emitting at 633 nm (adapted from the LuxiFlux™ device available from Hamamatsu) and equipped with interference bandpass filters (633BP10 nm from Schott) for a light illumination power of 15 μW/cm^2. The filtered fluorescence signal (filter RG665 from Schott) is measured by a cooled CCD camera (Orca II BT 512 G, Hamamatsu), placed at 160 mm from the imaging field, with an exposure time that is typically 20 ms. The Wasabi™ software (Hamamatsu) is used to drive the setup and for image processing. Fluorescence images can be superimposed on the black-and-white picture for better localization of the fluorescent signal. Semi-quantitative data can be obtained from the fluorescence images by drawing regions of interest (ROI) on the area to be quantified. The results are expressed as a number of relative light units per pixel.

3 Results and Discussion

3.1 *Encapsulation of Lipophilic Dialkylcarbocyanine Dyes in Lipid Nanoparticles*

Figure 2 depicts the structure of the dye-loaded LNPs. The LNP core is composed of a mixture of vegetable oil (from 0 to 75% w/w) and wax (Suppocire, from 25 to 100% w/w), to which can be mixed the DiD or DiR dyes (structures represented in Fig. 1). The presence of Suppocire allows the solubilization of a high concentration of lecithin (6.9% w/w for formulation A1, 5% w/w for formulations A2, B2, C2), which, in combination with polyoxyethylene (PEG) surfactants (11.4% w/w for formulation A1, 16.6% w/w for formulations A2, B2, C2), stabilizes very efficiently the droplets in aqueous buffer. Practically, the oily phase (oil, wax, lecithin, and eventually the DiD or DiR dye) is mixed with the aqueous phase (PEG surfactant, glycerol, buffer), and the microemulsion is sonicated to yield 35-nm-diam (formulation A1) or 30-nm-diam (formulations A2, B2, C2) LNPs. In this paper, we mainly focus on nanoparticles issued from the formulation A1 composed of 2.5% soybean oil, 7.5% Suppocire, 6.9% lecithin, 11.4% Myrj53 (PEG surfactant), 2.5% glycerol, 69.2% PBS (unless stated otherwise). The size of the particles is mainly governed by the nature, concentration, and ratio of the surfactants used. When increasing the ratio of the PEG-:lecithin surfactants from 33%:66% (formulation A1) up to 50%:50% (formulation A2), we observe a small decrease of the nanoparticle size (30 versus 35 nm). However, no significant differences are observed for formulations A2, B2, and C2, for which the core lipid content (oil/wax ratio) differs, but are processed using the same surfactant (PEG, lecithin) content. The typical dye concentration used is 400 μM, which corresponds to a number of 21 dyes/particle (35 nm diam). The efficient dialysis of the LNP dispersions ensures elimination of any nonincorporated molecules (dyes, surfactants) at the end of the process.

The absorption and emission spectra of the DiD and DiR fluorophores in methanol or encapsulated within the LNPs (formulation A1) are displayed in Fig. 3. No major modification is observed in the spectral properties of the dyes upon encapsulation (data, Table 1), except a slight increase of the 600-nm absorption band, possibly indicative of the presence of a few dye dimers. The absorption and emission maximum wavelengths of DiR and DiD are also very slightly redshifted (1–3 nm) upon encapsulation and are similar to those of their hydrophilic counterparts, respectively, Cy5 and Cy7 (Fig. 1, Table 1). For nondoped LNPs, it has to be noted that there is a continuous increase of the absorbance with decreasing wavelengths (Absorbance $\propto \lambda^{-4}$), as a slight Rayleigh scattering effect (Fig. 3). This effect is taken into account for the calculation of the fluorescence quantum yields of the encapsulated dyes.

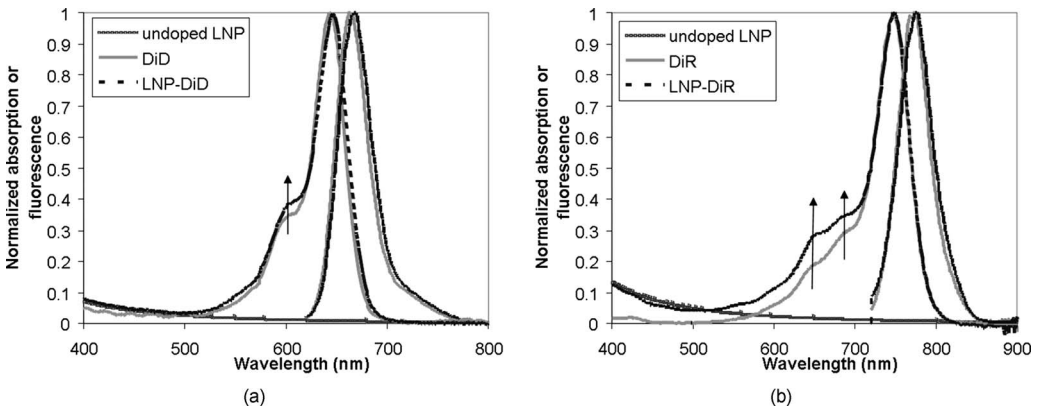

Fig. 3 Absorption and emission spectra of (a) DiD and (b) DiR in methanol or encapsulated within the LNPs, and absorption spectrum of the blank formulation (35-nm-diam particles; formulation A1 dispersed in 1 X PBS).

The perfect match of the absorption and emission spectra of the formulation before and after dialysis demonstrates the 100% efficiency of incorporation of the lipophilic cyanines in the LNPs, for total dye concentration in the dispersion in the range of 75–1000 μM. This corresponds to the incorporation of 4–53 dyes per particle, or a local dye concentration of 0.30–3.9 mM in the droplets. Figure 4(a) displays the hydrodynamic diameter of the nanoparticles either loaded or not by the fluorophores, measured by dynamic light scattering (DLS) in PBS buffer. For formulation A1, only one-sized population centered at 35 ± 2 nm is evidenced by DLS, with a very reproducible size polydispersity of 0.17. Whatever the oily core composition, only one-sized population centered at 30 ± 2 nm is evidenced by DLS for formulations A2, B2, and C2. However, the cryo-TEM image of Fig. 4(b) evidences different sizes and forms, which are attributed to oblong particles viewed from different angles. Platelet or oblong particles have also been observed by cryo-TEM in the case of solid LNPs dedicated to drug delivery.[45] In this work, we will describe the particle size by their mean DLS hydrodynamic diameter; moreover, only one population is observed by this technique. As already noted, modification of the oil/wax ratio of the LNP core does not modify the particle size, which is mainly governed by the surfactant properties, concentrations, and ratios.

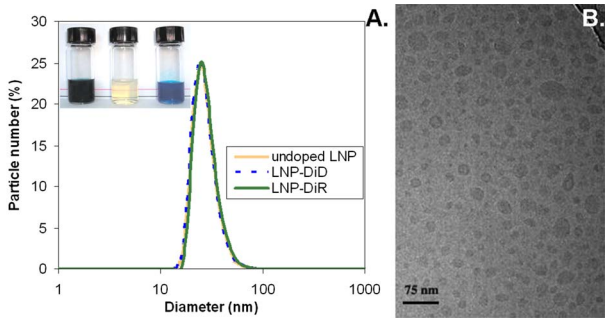

Fig. 4 (a) Size distribution of undoped and DiR- or DiD-loaded LNP measured by diffusion light scattering in 0.1 X PBS (formulation A1, 21 dyes/particle). The inset demonstrates the transparent aspect of the colloidal suspension because the particle diameter is <100 nm (left: DiR-loaded LNPs, middle: undoped particles; right: DiR-loaded LNPs). (b) Cryo-TEM image of undoped LNPs.

Similarly, the dye encapsulation does not modify the droplet diameter, neither their zeta potential, which remains neutral (-5 ± 2 mV). The neutrality of the surface of the particles is certainly ensured by the use of zwitterionic lecithin and neutral PEG surfactants. The fact that the LNP surface remains neutral despite the positively charged dye encapsulation confirms that the fluorophores are encapsulated within the lipid core rather than adsorbed on, or included in, the particle surfactant surface.

3.2 *Stability of Dye-Loaded Lipid Nanoparticles*

The inset in Fig. 4(a) demonstrates the transparent aspect of the colloidal suspension since the particle diameter is <100 nm. The transparency of the solution is therefore a good indicator of its colloidal stability. Fluorescence and colloidal stabilities of 21 DiD/particle LNP dispersions (formulation A1) prepared at pH 5.5 in HBS buffer (HEPES 0.02 M; EDTA 0.01 M) and kept protected from light on the laboratory shelf are further assessed by DLS and fluorescence measurements [Fig. 5(a)]. A very good stability of both the fluorescence properties of the encapsulated dyes and the size of the droplets is observed for more than one year in HBS buffer. This stability is observed in the pH 3–8 range (adjusted by NaOH or HCl), either in water, PBS, or HBS buffers, for at least 100 days. However, the fluorescence properties of DiD-loaded LNP become altered rapidly in basic medium (pH >8) [Fig. 5(b)]. The colloidal stability of the solution is maintained, but its color shifts from blue to green and yellow. The loss of fluorescence signal can therefore be accounted for by a chemical degradation of the cyanine dye, a class of fluorophores known to be sensitive to pH conditions.[18] This is confirmed by the disappearance of the 646-nm absorption band of the dye and the appearance of a new absorbance band at 467 nm, associated with a weak emission centered at 497 nm. On the contrary, in acidic media, the loss of the fluorescence properties, which occurs on a longer time scale [Fig. 5(b)], goes along with the appearance of opaqueness of the dispersions. In this case, the absorption spectra of the LNPs always display the absorption and emission bands of the DiD dye with reduced intensities, but also an important increased scattering: there exist both a degradation of the fluorophore (but different from in basic media because no

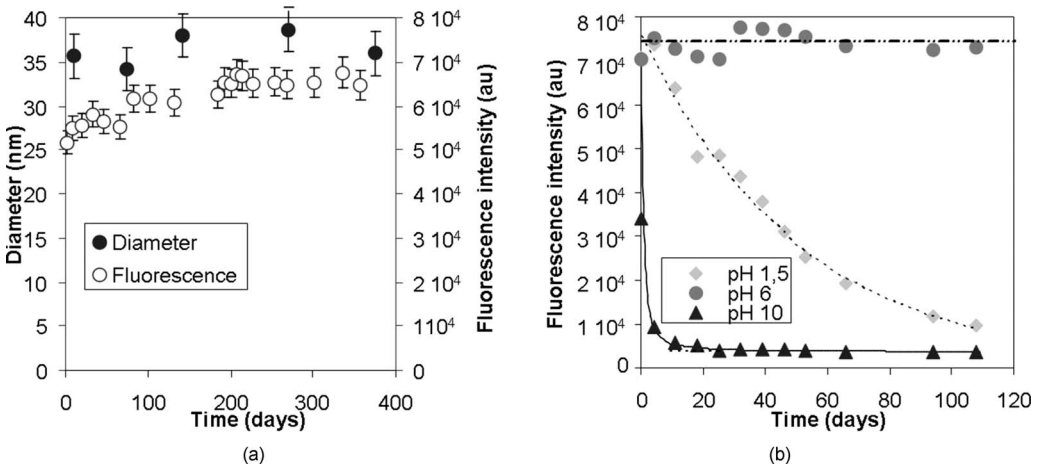

Fig. 5 (a) Colloidal and fluorescence stability of DiD-loaded LNP (formulation A1, 21 dyes/particle) dispersed in HBS buffer (Hepes 0.02 M, EDTA 0.01 M, pH 5.5). (b) Fluorescence stability of DiD-loaded LNPs (formulation A1, 21 dyes/particle) in deionized water added by concentrated HCl or NaOH to adjust the pH.

color change is observed) and a destabilization of the nanoparticles.

Figure 6 displays the evolution of the fluorescence of the DiD fluorophore in methanol or encapsulated in LNPs, in comparison to that of its hydrophilic counterpart (Cy5) whenever submitted to a continuous light irradiation at 633 nm for 24 h (excitation power: 200 μW/cm^2). The photobleaching rate of DiD-loaded LNPs dispersed in aqueous buffer is higher than for the free dye in methanol. Moreover, this photobleaching rate is slightly sensitive to the continuous medium (154 mM NaCl or 1X PBS buffers) in which the particles are dispersed. However, this photobleaching rate is far reduced in comparison to that of Cy5 dissolved in the same buffers.

Because dye degradation is observed in basic buffer, and the fluorophore photobleaching kinetics is sensitive to the continuous phase, it might be indicative that despite its LNP encapsulation, the fluorophore might exchange with the continuous medium. This could be due to the nature of the LNPs, which are permeable and deformable nanoparticles, the fluid surfactant interface through which oxygen and ions could diffuse. The increased photobleaching observed in the LNP core in comparison to the free dye in methanol could also be due to possible photoreactions occurring between the dye in its excited state and the lipid components composing the LNP core. In particular, soybean oil is mainly constituted from unsaturated glycerides, which might be prone to oxydation. However, all previous results (Fig. 5) demonstrate the very good encapsulation and stability of the lipophilic dialkylcarbocyanine dyes in the LNP in the pH 3–8 range, compatible with *in vivo* conditions. This is certainly due to the choice of the fluorophores, with long lipophilic chains (Fig. 1), which confer them a very good affinity for the lipid core of the droplets.

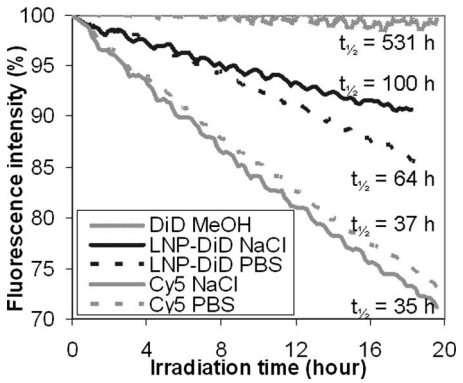

Fig. 6 Compared photobleaching of Cy5, DiD, and DiD-loaded LNPs (formulation A1, 21 dyes/particle, 154 mM NaCl or 1X PBS (10 mM phosphate, 137 mM NaCl, 2.7 mM KCl, pH 7.4)). The excitation wavelength is 633 nm, and the excitation power 200 μW/cm^2. Half-lives ($t_{1/2}$) of the dyes, calculated using a linear fit of the curves, are indicated.

3.3 *Fluorescence Quantum Yields and Lifetimes of Dye-Loaded Lipid Nanoparticles*

The fluorescence quantum yields and lifetimes of the DiD and DiR dyes, either in methanol or encapsulated in the LNP of different formulations, as well as those of their hydrophilic counterparts Cy5 and Cy7 in PBS buffer are listed in Table 1. As already noted, both the fluorescence quantum yields and lifetimes decrease when shifting from the red part (Cy5 and DiD) to the near-infrared part (Cy7 and DiR) of the spectrum. The role of the buffer on these optical parameters is also very important: despite very similar structures, Cy5 (respectively, Cy7) dispersed in an aqueous buffer displays lower fluorescence quantum yield than DiD (respectively, DiR) dispersed in methanol (DiD and DiR are not soluble in water or aqueous buffers). These lower performances of organic dyes in aqueous media are often accounted for by fluorescence quenching of buffer components, limited dye solubility or dye aggregation, or the presence of oxygen, which is known, in particular, to favor dye photobleaching.

However, it is necessary for biological applications and especially for *in vivo* imaging in animals to dispose of efficient fluorescent tracers with optimized optical properties in aqueous buffers, compatible with injection. Therefore, the encapsulation of dyes within "organiclike" medium nanoparticles, in which they could display improved optical proper-

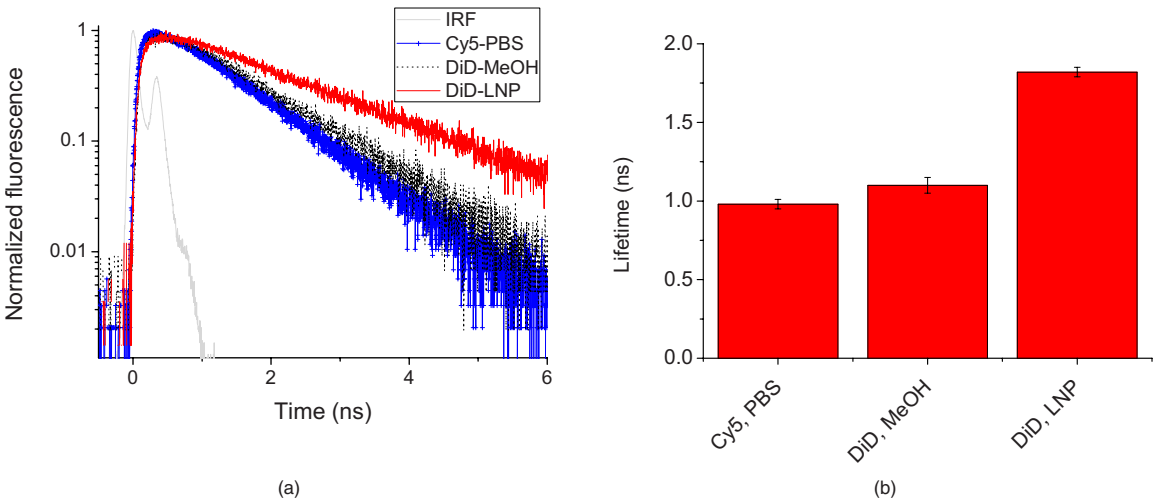

Fig. 7 (a) Fluorescence decays and (b) lifetimes of Cy5 (1X PBS), DiD (MeOH), and DiD-loaded LNP (1X PBS, formulation A1, 21 dyes/particle). The excitation wavelength is 630 nm.

ties, is attractive if these nanoparticles can be dispersed with a good colloidal stability in water. LNPs respond to this demand. Indeed, DiD and DiR encapsulated within LNPs display fluorescence quantum yields and lifetimes similar or even higher than the free dyes dispersed in organic solution (Table 1, Fig. 7). A high dye loading ratio can be achieved (>99 % encapsulation efficiency, up to at least 53 dyes per 35 nm diameter particle, corresponding to a dye local concentration of 3.9 mM), without any significant fluorescence auto-quenching (Table 1). This is noticeable since cyanines are known to be prone to aggregation and auto-quenching in aqueous buffers.[18] Therefore, DiD and DiR loading within LNP provides aqueous soluble fluorescent labels with far improved fluorescence quantum yields Φ (respectively 0.38 and 0.25) and longer fluorescence lifetimes τ (respectively 1.8 ns and 1.1 ns) in comparison to their hydrophilic counterparts Cy5 (Φ=0.28, τ=1.0 ns) and Cy7 (Φ=0.13, τ=0.57 ns) (Table 1, Figure 7). Moreover, very high global dye concentrations (at least 1 mM in water) can be achieved without any solubility problem or deterioration of the optical properties due to aggregation, contrary to the direct solubilization of hydrophilic cyanines in water.

We also notice that the fluorescence quantum yield and lifetime of DiD whenever encapsulated in the LNP are increased in comparison to those of the free dye in methanol (Table 1). In order to better understand the LNP encapsulation effects on the dye photophysics, radidative $[k_r=(\Phi/\tau)]$ and nonradiative $[k_{nr}=(1-\Phi)/\tau]$ rate constants derived from steady-state and time-resolved experiments are listed in Table 1. Fluorescence quantum yields and lifetimes are dependant on both the radiative and nonradiative processes. Larson et al. reported a 2.2-fold increase of the radiative rates of TRITC (a rhodamine dye) upon silica encapsulation, relatively to water.[37] They account for this increase of the radiative rates by the change of refractive index between silica (n=1.46) and water (n=1.33), according to a model described by Toptygin et al.[46] On the contrary, in this study, for a similar change of the refractive index between soybean oil (n=1.47) and methanol (n=1.33), a decrease of the radiative rate of DiD and DiR is observed. The radiative rate modifications observed in this study should therefore be attributed to other interactions between the dyes and the lipid matrix.

Nonradiative decays can be accounted for by three process: (*i*) intersystem conversion from the excited singlet state to the triplet; (*ii*) photoisomerization, which is a well-acknowledged process for cyanine dyes,[18] and (*iii*) internal conversion closely linked to the vibrational and rotational degrees of freedom of the dyes. Intersystem conversion has been reported as negligible for cyanine dyes in the absence of heavy atoms.[47] Photoisomerization and internal conversion are both influenced by the polarity and viscosity of the dye-surrounding medium. Two studies carried out on several tricarbocyanines in solvents of different polarities and viscosities attributed the decrease of radiative rates observed in nonpolar media in comparison to more polar solvents mainly to polarity effects, with low-viscosity influence.[47,48] On the contrary, other studies point out the importance in the nonradiative decay rates of the dye rotational degrees of freedom, which is linked to the viscosity.[18,37] In particular, Larson et al. reported that the nonradiative rate constants of a rhodamine dye in a silica matrix is directly linked to the rotational mobility of the fluorophore.[37] The less movement the dye can have, the slower the nonradiative decay is. LNPs display both a high viscosity (79 cP for soybean oil, Suppocire is solid at 25 °C) and a very low polarity (solvent orientation polarizability as defined in Ref. 48 is Δf=0.06–0.09 for soybean oil) in comparison to methanol (0.58 cP, Δf=0.31). Therefore, both effects could explain the decrease of the nonradiative rate observed for DiD from methanol to LNPs. The fact that no significant difference is observed between the nonradiative rates for the different A2, B2, and C2 formulations, which display different wax contents and therefore different viscosities, seems to indicate that the modification of the nonradiative rate observed between methanol and the LNP should be due mainly to a polarity effect. Surprisingly, no significant difference is observed for the DiR dye between methanol and the LNP core in comparison to what is observed for DiD.

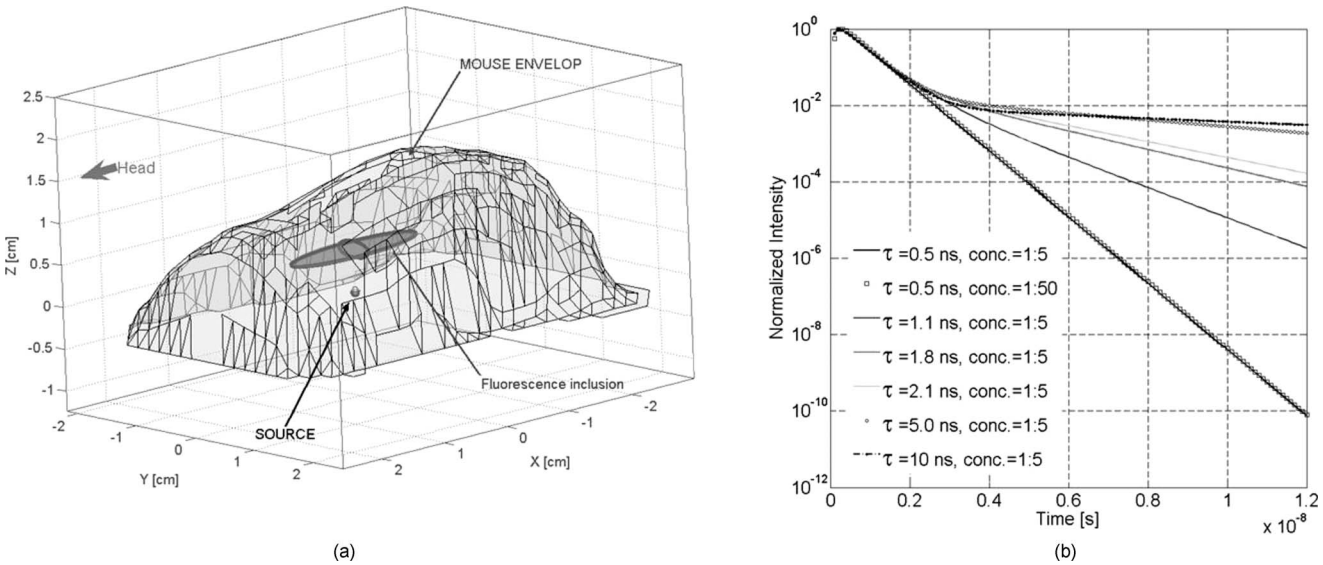

Fig. 8 (a) Description of the synthetic mouselike medium used for simulations: it is composed of three subdomains, representing the body of the mouse, the ellipsoidal fluorescence inclusion, and the position of the excitation source. (b) Temporal fluorescence profiles detected at position (0.2, 0, 0.25 cm), for different relative fluorochromes concentrations (conc. background:inclusion), and increasing inclusion lifetime τ (background lifetime is kept unchanged and equal to 0.5 ns).

Figure 8(b) displays the temporal fluorescence profiles simulated for a dye inclusion placed in the 3-D digitized volume of a living mouse [geometry described in Fig. 8(a)].[42] The results represent the normalized intensities measured at position (0.2,0,0.25), for a simulated reflection detection mode. The same kind of curves have been obtained for simulated transmission acquisitions. The calculations are performed for different relative background to inclusion concentrations (background:inclusion 1:5 or 1:50), and for different values of the inclusion lifetime, corresponding to the same lifetime as the background (0.5 ns), DiD in MeOH (1.1 ns), DiD in A1 formulated LNPs (1.8 ns), and DiD in B2-C2 formulated LNPs (2.1 ns). Longer lifetimes (5 and 10 ns) have also been considered. A first global remark is that the curves, plotted with a logarithmic scale, highlight two distinct behaviors: for short times (basically, >0.1 and <0.3 ns), the slope of the linear curve is equal to the inverse of the background lifetime, and at long times, to the inverse of the inclusion lifetime. Hence, by time gating the measured signal, one could selectively decouple the signal coming from the background and the signal coming actually from the ROI. Increasing the concentration of the fluorescence inclusion (conc. 1:5 to conc. 1:50) does not exhibit any difference in the time profiles, the modifications appear only on the level of signal detected. On the contrary, increasing the inclusion lifetime allows an easier detectability of the molecular probes. Nevertheless, if the lifetimes are too long (>5 ns), it becomes difficult to exploit the slope of the curves (almost horizontal) to identify the marker through its lifetime.

To summarize, developing fluorescence molecular probes with lifetimes in the 1.0–3.0 ns range provides two major advantages: (*i*) possibility of time gating the fluorescence signal in order to selectively measure the emitted photons coming from the targeted zone; (*ii*) identifying the fluorochromes through the slope of the logarithmic curves at long times. In this perspective, DiD- and DiR-loaded LNPs (respectively, 1.8 and 1.1 ns) appear more interesting labels in comparison to their classical water soluble counterparts Cy5 and Cy7 (respectively, 1.0 and 0.57 ns). Moreover, DiD lifetimes appear to be sensitive to the LNP dye encapsulation. Therefore, in addition to its use as an imaging agent, DiD-loaded LNPs could be an interesting system to model and investigate the release of a lipophilic drug from the LNP carrier.

3.4 *Passive Tumor Targeting of Dye-Loaded LNP*

Preliminary *in vivo* experiments are undertaken in order to demonstrate the potential of the new LNP nanocarriers for fluorescence imaging and other potential diagnostic and therapeutic applications. First, DiD-loaded LNPs [5×10^{14} particles (3.2 mg of oil) at a local DiD concentration of 1.55 mM, dispersed in 200 μL of 1X PBS buffer, corresponding to 10 nmol of dye] are injected intravenously in healthy Nude mice ($n=4$). The fluorescence signal distributes very rapidly in the whole animal, and 24 h after injection, no organ seems to preferentially accumulate the dye (Fig. 9). This is outstanding because most nanocarriers of similar size can be quite rapidly uptaken by the macrophages of the reticuloendothelial system [(RES): mainly liver, spleen, bone marrow] after plasma protein binding.[49] The high density in the LNP shell of surfactants with a polyoxyethylene chain (PEG), which has been demonstrated to considerably reduce nanoparticle protein adsorption and therefore increase the plasma half-life of various nanocarriers, is certainly very important for conferring the LNP this suitable pharmacokinetics.[50–52] Because of their very probable long lifetime circulation, efficient passive tumor accumulation of the LNPs in cancer models displaying leaky fenestrations should be achieved due to the EPR effect.[33] Ts/Apc ($n=4$) and OVCAR-3 ($n=2$) xenografted model mice have been used for imaging the passive tumor uptake of DiD-loaded LNPs. Ts/Apc (murine breast cancer model) and OVCAR-3 (human ovarian adenocarci-

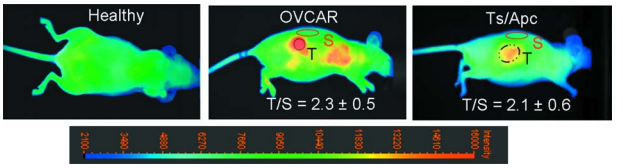

Fig. 9 *In vivo* imaging with DiD-loaded LNPs (formulation A1, 21 dyes/particle). Fluorescence images obtained 24 h after injection of DiD-loaded LNPs (3.2 mg of oil, 10 nmol of DiD in 200 μL PBS buffer) in nude mice, either healthy or bearing xenografted subcutaneous tumors. Fluorescence images (in color scale, lower part of the figure) are superimposed to visible light images (in white and black). For fluorescence images, the integration time is 20 ms and the contrast has been set between 2100 and 16,000. The tumor-over-skin ratio has been calculated by drawing a region of interest and quantifying the fluorescence signal with the Wasabi™ software. (Color online only.)

noma model) are tumor cells with a fast growth, leading to an imperfect vascular endothelium with leaky fenestrations. Figure 9 displays the fluorescent images obtained 24 h after intravenous injection in tail of DiD-loaded LNPs at the same dose than for a healthy animal (10 nmol of dye, 5×10^{14} particles dispersed in 200 μL 1X PBS) for the two different tumor models. A significant accumulation (tumor/skin fluorescence ratio=2.1–2.3) is observed for both the Ts/Apc (n=4) and OVCAR-3 (n=2) models; 24 h corresponds to the time after injection for which the tumor fluorescence intensity as well as the tumor/skin fluorescence ratio are maximum in the two models. These preliminary experiments therefore demonstrate the possibility to use DiD-loaded LNPs for passive tumor uptake and imaging.

4 Conclusions

New LNPs based on the use of cheap GRAS components and able to encapsulate with a >99% efficiency near-infrared lipophilic cyanines for *in vivo* imaging purposes are described. They display ≈30–35 nm hydrodynamic diameter and a very long colloidal stability (>1 y) at room temperature in aqueous buffer. In comparison to other organic nanocarriers, such as liposomes, LNPs allow the encapsulation of high quantities of lipophilic compounds and are far more stable: LNP can be stored in injection-ready formulations for a long duration.

Thanks to their nonpolar core, LNPs provide a suitable medium for conferring to the dyes outstanding optical properties, while dispersed in aqueous buffers. Fluorescence quantum yields as high as 38% for DiD-loaded LNPs and 25% for DiR-loaded LNPs have been achieved, which is the best fluorescence quantum yields reported for fluorescent labels dispersed in aqueous buffers in these wavelength range, to our knowledge. Moreover, these very bright labels also have long fluorescence lifetimes, which should present a tremendous advantage for time-resolved fluorescence imaging.

The nanocharacter of these labels can be exploited for *in vivo* tumor imaging, taking benefit of the EPR effect. Further *in vivo* experiments are under course, but we can already envision that these new nanoparticles, manufactured by an easily scaled-up process based on the use of natural and cheap components, will pave the way to a new generation of fluorescent nanomarkers.

Acknowledgments

We thank Thomas Delmas for help during the fluorescence lifetime measurements. This work was supported by the Commissariat à l'Energie Atomique and the French National Research Agency (ANR) through Carnot funding and Contract No ANR-08-NANO-006-02.

References

1. S. Gross and D. Piwnica-Worms, "Molecular imaging strategies for drug discovery and development," *Curr. Opin. Chem. Biol.* **10**, 334–346 (2006).
2. K. Licha and C. Olbrich, "Optical imaging in drug discovery and diagnostic applications," *Adv. Drug Delivery Rev.* **57**, 1087–1108 (2005).
3. J. Willmann, N. van Bruggen, L. M. Dinkelborg, and S. S. Gambhir, "Molecular imaging in drug development," *Nat. Rev. Drug Discovery* **7**, 591–607 (2008).
4. J. V. Frangioni, "New technologies for human cancer imaging," *J. Clin. Oncol.* **26**(24), 4012–4021 (2008).
5. E. M. Sevick-Muraca and J. C. Rasmussen, "Molecular imaging with optics: primer and case for near-infrared fluorescence techniques in personalized medicine," *J. Biomed. Opt.* **13**(4), 041303 (2008).
6. R. Weissleder and M. J. Pittet, "Imaging in the era of molecular oncology," *Nature (London)* **452**, 580–589 (2008).
7. I. L. Medintz, H. Mattoussi, and A. R. Clapp, "Potential clinical applications of quantum dots," *Int. J. Nanomed.* **3**(2), 151–167 (2008).
8. X. Michalet, F. F. Pinaud, L. A. Bentolila, J. M. Tsay, S. Doose, J. J. Li, G. Sundaresan, A. M. Wu, S. S. Gambhir, and S. Weiss, "Quantum dots for live cells, *in vivo* imaging, and diagnostics," *Science* **307**(5709), 538–544 (2005).
9. A. M. Smith, H. Duan, A. M. Mohs, and S. Nie, "Bioconjugated quantum dots for *in vivo* molecular and cellular imaging," *Adv. Drug Delivery Rev.* **60**, 1226–1240 (2008).
10. J. V. Frangioni, "*In vivo* near-infrared fluorescence imaging," *Curr. Opin. Chem. Biol.* **7**, 626–634 (2003).
11. M. S. T. Gonçalves, "Fluorescent labeling of biomolecules with organic probes," *Chem. Rev. (Washington, D.C.)* **109**(1), 190–212 (2009).
12. S. A. Hilderbrand, K. A. Kelly, R. Weissleder, and C. H. Tung, "Monofunctional near-infrared fluorochromes for imaging applications," *Bioconjugate Chem.* **16**(5), 1275–1281 (2005).
13. H. Lee, C. Mason, and S. Achilefu, "Heptamethine cyanine dyes with a robust C-C bond at the central position of the chromophore," *J. Org. Chem.* **71**(20), 7862–7865 (2006).
14. K. Licha, "Contrast agents for optical imaging," in *Contrast Agents LI*, pp. 1–29, Springer-Verlag, Berlin (2002).
15. W. Pham, Z. Medarova, and A. Moore, "Synthesis and application of a water-soluble near-infrared dye for cancer detection using optical imaging," *Bioconjugate Chem.* **16**(3), 735–740 (2005).
16. Y. Ye, S. Bloch, J. Kao, and S. Achilefu, "Multivalent carbocyanine molecular probes: synthesis and applications," *Bioconjugate Chem.* **16**(1), 51–61 (2005).
17. Z. Zhang and S. Achilefu, "Synthesis and evaluation of polyhydroxylated near-infrared carbocyanine molecular probes," *Opt. Lett.* **6**(12), 2067–2070 (2004).
18. A. Mishra, R. K. Behera, P. K. Behera, B. K. Mishra, and G. B. Behera, "Cyanines during the 1990s: a review," *Chem. Rev. (Washington, D.C.)* **100**, 1973–2011 (2000).
19. H. Lee, M. Y. Berezin, M. Henary, L. Strekowski, and S. Achilefu, "Fluorescence lifetime properties of near-infrared cyanine dyes in relation to their structures," *J. Photochem. Photobiol., A* **200**, 438–444 (2008).
20. E. Arunkumar, C. C. Forbes, and B. D. Smith, "Improving the optical properties of organic dyes by molecular encapsulation," *Eur. J. Org. Chem.* 4051–4059 (2005).
21. S. A. Hilderbrand, K. Kelly, M. Niedre, and R. Weissleder, "Near infrared fluorescence-based bacteriophage particles for ratiometric pH imaging," *Bioconjugate Chem.* **19**, 1635–1639 (2008).
22. P. Ghoroghchian, P. Frail, K. Susumu, D. Blessington, A. Brannan, F. Bates, B. Chance, D. Hammer, and M. Therien, "Near IR emissive polymersome: self-assembled soft matter for *in vivo* optical imaging," *Proc. Natl. Acad. Sci. U.S.A.* **102**(8), 2922–2927 (2004).

23. I. R. Corbin, J. Chen, W. Cao, H. Li, S. Lund-Katz, and G. Zheng, "Enhanced cancer-targeted delivery using engineered high-density lipoprotein-based nanocarriers," *Biomed. Tech.* **3**, 367–376 (2007).
24. A. Almutairi, W. J. Akers, M. Y. Berezin, S. Achilefu, and J. M. J. Fréchet, "Monitoring the biodegradation of dendritic near-infrared nanoprobes by *in vivo* fluorescence imaging," *Mol. Pharmacol.* **5**(6), 1103–1110 (2008).
25. M. A. Quadir, M. R. Radowski, F. Kratz, K. Licha, P. Hauff, and R. Haag, "Dendritic multishell architectures for drug and dye transport," *J. Controlled Release* **132**, 289–294 (2008).
26. V. Deissler, R. Rüger, W. Frank, A. Fahr, W. A. Kaiser, and I. Hilger, "Fluorescent liposomes as contrast agents for *in vivo* optical imaging of edemas in mice," *Small* **4**(8), 1240–1246 (2008).
27. A.-K. Kirchherr, A. Briel, and K. Mäder, "Stabilization of indocyanine green by encapsulation within micellar systems," *Mol. Pharmacol.* **6**(2), 480–491 (2009)
28. A. L. Doiron, K. A. Homan, S. Emelianov, and L. Brannon-Peppas, "Poly(lactic-co-glycolic) acid as a carrier for imaging contrast agents," *Pharm. Res.* **26**(3), 674–682 (2009).
29. H. Tanisaka, S. Kizaka-Kondoh, A. Makino, S. Tanaka, M. Hiraoka, and S. Kimura, "Near-infrared fluorescent labeled peptosome for application to cancer imaging," *Bioconjugate Chem.* **19**, 109–117 (2008).
30. E. I. Altinoglu, T. J. Russin, J. M. Kaiser, B. M. Barth, P. C. Eklund, M. Kester, and J. H. Adair, "Near-infrared emitting fluorophore-doped calcium phosphate nanoparticles for *in vivo* imaging of human breast cancer," *ACS Nano* **2**(10), 2075–2084 (2008).
31. A. Burns, H. Ow, and U. Wiesner, "Fluorescent core-shell silica nanoparticles: towards "lab on a particle" architectures for nanobiotechnology," *Chem. Soc. Rev.* **35**, 1028–1042 (2006).
32. S. Kumar, I. Roy, T. Y. Ohulchanskyy, L. N. Goswani, A. C. Bonoiu, E. J. Bergey, K. M. Tramposch, A. Maitra, and P. Prasad, "Covalently dye-linked, surafce-controlled, and bioconjugated organically modified silica nanoparticles as targeted probes for optical imaging," *ACS Nano* **2**(3), 449–456 (2008).
33. H. Maeda, J. Wu, T. Sawa, Y. Matsumura, and K. Hori, "Tumor vascular permeability and the EPR effect in macromolecular therapeutics: a review," *J. Controlled Release* **65**, 271–284 (2000).
34. P. Carmeliet and R. K. Jain, "Angiogenesis in cancer and other diseases," *Nature (London)* **407**, 249–257 (2000).
35. P. Decuzzi, R. Pasqualini, W. Arap, and M. Ferrari, "Intravascular delivery of nanoparticulate systems: does geometry really matter?," *Pharm. Res.* **26**(1), pp. 235–243 (2008).
36. J. F. Bringley, T. L. Penner, R. Wang, J. F. Harder, W. J. Harrison, and L. Buonemani, "Silica nanoparticles encapsulating near-infrared emissive cyanine dyes," *J. Colloid Interface Sci.* **320**, 132–139 (2008).
37. D. R. Larson, H. Ow, H. D. Vishwasrao, A. A. Heikal, U. Wiesner, and W. W. Webb, "Silica nanoparticle architecture determines radiative properties of encapsulated fluorophores," *Chem. Mater.* **20**, 2677–2684 (2008).
38. E. Rampazzo, S. Bonacchi, M. Montalti, L. Prodi, and N. Zaccheroni, "Self-organizing core-shell nanostructures: spontaneous accumulation of dye in the core of doped silica nanoparticles," *J. Am. Chem. Soc.* **129**(46), 14251–14256 (2007).
39. S. Santra, B. Lisenfeld, C. Bertolino, D. Dutta, Z. Cao, W. Tan, B. Moudgil, and R. Mericle, "Fluorescence lifetime measurements to determine the core-shell nanostructure of FITC-doped silica nanoparticles: an optical approach to evaluate nanoparticle photostability," *J. Lumin.* **117**, 75–82 (2006).
40. R. Sens and K. H. Drexhage, "Fluorescence quantum yield of oxazine and carbazine laser dyes," *J. Lumin.* **24–25**(Part 2), 709–712 (1981).
41. J. X. Duggan, J. DiCesare, and J. F. Williams, "Investigations on the use of laser dyes as quantum counters for obtaining corrected fluorescence spectra in the near infrared," in *New Directions in Molecular Luminescence E. ASTM STP 822*, D. Eastwood, Ed., pp. 112–126, American Society for Testing and Materials (1983).
42. A. Koenig, L. Hervé, J. Boutet, M. Berger, J.-M. Dinten, A. Da Silva, P. Peltié, and P. Rizo, "Fluorescence diffuse optical tomographic system for arbitrary shaped small animals," in *5th IEEE International Symposium on Biomedical Imaging—From Nano to Micro*, Paris, pp. 1593–1596 (2008).
43. C. L. Hutchinson, J. R. Lakowicz, and E. M. Sevick-Muraca, "Fluorescence lifetime based sensing in tissues: a computational study," *Biophys. J.* **68**, 1574–1582 (1995).
44. National Institutes of Health, "Principles of laboratory animal care," NIH Pub. No. 86–23, revised (1985).
45. W. Mehnert and K. Mäder, "Solid lipid nanoparticles: production, characterization and applications," *Curr. Opin. Chem. Biol.* **47**, 165–196 (2001).
46. D. Toptygin, R. S. Savtchenko, N. D. Meadow, S. Roseman, and L. Brand, "Effect of the solvent refractive index on the excited-state lifetime of a single tryptophan residue in a protein," *J. Phys. Chem. B* **106**, 3724–3734 (2002).
47. S. A. Soper and Q. L. Mattingly, "Steady-state and picosecond laser fluorescence studies of non radiative pathways in tricarbocyanine dyes: implications to the design of near-IR fluorochromes with high fluorescence intensities," *J. Am. Chem. Soc.* **116**, 3744–3752 (1994).
48. M. Y. Berezin, H. Lee, W. J. Akers, and S. Achilefu, "Near infrared dyes as lifetime solvatochromic probes for micropolarity measurements of biological systems," *Biophys. J.* **93**, 2892–2899 (2007).
49. P. Couvreur and C. Vauthier, "Nanotechnology: intelligent design to treat complex disease," *Pharm. Res.* **23**(7), 1417–1450 (2006).
50. M. Hamidi, A. Azadi, and P. Rafiei, "Pharmacokinetic consequences of Pegylation," *Drug Deliv.* **13**, 399–409 (2006).
51. S. M. Moghimi, A. C. Hunter, and J. C. Murray, "Long-circulating and target-specific nanoparticles: theory to practice," *Pharmacol. Rev.* **53**(2), 283–318 (2001).
52. C. Monfardini and F. M. Veronese, "Stabilization of substances in circulation," *Bioconjugate Chem.* **9**, 418–450 (1998).